Chapter 8
Modal Analysis of Rotating Wind Turbine Using Multiblade Coordinate Transformation and Harmonic Power Spectrum

Shifei Yang, Dmitri Tcherniak, and Matthew S. Allen

Abstract Understanding and characterization of wind turbine dynamics, especially when operating, is an important though challenging task. The main problem is that an operating wind turbine cannot be truly modeled as a time invariant system, which limits the applicability of conventional well-established modal analysis methods. This paper compares two experimental techniques that characterize the dynamic behavior of an operating horizontal axis wind turbine (Vestas V27, 225 kW, rotor diameter 27 m, 12 accelerometers on each blade). The first method uses a multiblade coordinate transformation to convert the time periodic system into a time invariant one, assuming that the system is perfectly isotropic. Conventional operational modal analysis then can be applied to identify the modal parameters of the time invariant model. The second method processes the periodic response directly based on an extension of modal analysis to linear time periodic systems. It utilizes the harmonic power spectrum, which is analogous to the power spectrum for a time invariant system, to identify a periodic model for the turbine. This work demonstrates both of these methods on measurements from the operating turbine and discusses the challenges that are encountered. The procedure is demonstrated by using it to extract the time-periodic mode shapes of the first edge-wise modes, revealing that this turbine apparently has non-negligible blade-to-blade variations and hence the dynamics of these modes are considerably different than one would expect for an anisotropic turbine.

Keywords Linear time periodic • Output-only modal analysis • Wind turbine • Anisotropic • Dynamics

8.1 Introduction

The design of modern wind turbines heavily relies on accurate numerical models, which are used extensively to simulate the dynamic behavior of the wind turbines under different operating conditions. As a consequence, good experimental tools are necessary to validate the numerical models. However, it is quite challenging to experimentally characterize the dynamics of a wind turbine, especially when it is operating. One significant challenge is that many real turbines cannot be adequately modeled as a Linear Time Invariant (LTI) because of blade-to-blade variations, stratification in the flow field, and rotation of the rotor. If the angular speed of the rotor is constant then a wind turbine might be modeled as a Linear Time Periodic (LTP) system in order to characterize its behavior. This requires other methods, different from the conventional well-established modal analysis methods that are normally used for LTI systems.

This paper compares two experimental techniques for identifying wind turbines; the multiblade coordinate (MBC) transformation and the harmonic power spectrum. The MBC transformation, also known as the Coleman transformation, was first introduced in [1]. The idea behind the MBC transformation is to substitute the deflections of the blades measured in the blade coordinate system by some special variables, which combine the deflections of all three blades. MBC transformation results in elimination of the periodic terms in the equations of motion, thus making the system time invariant so that conventional modal analysis techniques can be applied. A fundamental requirement for the MBC transformation is that

S. Yang (✉) • M.S. Allen
Department of Engineering Physics, University of Wisconsin, Madison, WI, USA
e-mail: shifeiy@gmail.com; msallen@engr.wisc.edu

D. Tcherniak
Brüel & Kjær SVM, Nærum, Denmark
e-mail: dmitri.tcherniak@bksv.com

J. De Clerck (ed.), *Topics in Modal Analysis I, Volume 7: Proceedings of the 32nd IMAC, A Conference and Exposition on Structural Dynamics, 2014*, Conference Proceedings of the Society for Experimental Mechanics Series,
DOI 10.1007/978-3-319-04753-9_8,

the rotor is isotropic [2], namely that all blades are identical and symmetrically mounted on the hub. When focusing on experimental techniques, it is also necessary that measurement system is symmetric, i.e. the sensors are mounted identically on all three blades [3]. In a prior work, Tcherniak et al. used the MBC transformation on simulated wind turbine data in order to obtain a wind turbine Campbell diagram, i.e. a graph presenting the dependency of the modal parameters on the rotor speed [4].

The second method, the harmonic transfer function for linear time periodic systems, was developed to process the response of the linear time periodic system directly [5]. It is known that when a single frequency input is applied to an LTI structure, the response will be at the same frequency but with a different phase and amplitude. In contrast, the response of an LTP system will contain a component at the excitation frequency as well as at an infinite number of its harmonics, separated by an integer multiple of rotation frequency. The harmonic transfer function is analogous to the transfer function of a time invariant system, but relates the exponentially modulated input (i.e., an input signal described by a central frequency and a series of equally spaced harmonics) to the exponentially modulated output at the same collection of frequencies. Allen et al. extended the harmonic transfer function to the case where the input cannot be directly measured by introducing the harmonic power spectrum [6], and the modal parameters of a 5 MW turbine were identified from simulated data. Later, the harmonic power spectrum was combined with continuous-scan laser Doppler vibrometry, measuring the first few mode shapes along a single blade of a parked 20 kW wind turbine under wind excitation [7].

In this work, both the MBC transformation and harmonic power spectrum were employed to process measurements from an operating turbine under wind excitation. First, the formulation of *modes* of an LTV system used in both methods is discussed and compared. Then, the methods are applied to a horizontal axis wind turbine (Vestas V27, 225 kW, rotor diameter 27 m), which was instrumented with accelerometers on three blades and in the nacelle [3]. The identified modal parameters from both methods are discussed and compared to evaluate their validity. The rest of this paper is organized as follows: Sect. 8.2 introduces the theoretical basis for the MBC transformation and the harmonic power spectrum; Sect. 8.3 introduces the wind turbine and sensor arrangement. Sections 8.4–8.6 demonstrate the analysis applied to the data; Sect. 8.7 summarizes the paper.

8.2 Theory

8.2.1 Multiblade Coordinate Transformation

A multiblade coordinate transformation (MBC) is typically used to convert degrees of freedom (DOFs) measured on the blades, i.e. in the rotating frame, to a non-rotating frame [8], making it possible to combine the blade DOFs with those on the tower and the nacelle. In the case of a three-bladed rotor, the sets of three coordinates $\{q_{1,k}\,, q_{2,k}\,, q_{3,k}\}^{\mathrm{T}}$ measured at the position k on blades 1, 2, 3 will be converted to the sets of three multiblade coordinates $\{a_{0,k}\,, a_{1,k}\,, b_{1,k}\}\}^{\mathrm{T}}$ given by

$$a_{0,k} = \tfrac{1}{3}\sum_{i=1}^{3} q_{i,k}, \quad a_{1,k} = \tfrac{2}{3}\sum_{i=1}^{3} q_{i,k}\cos\phi_i, \quad b_{1,k} = \tfrac{2}{3}\sum_{i=1}^{3} q_{i,k}\sin\phi_i, \tag{8.1}$$

where ϕ_i is the instantaneous azimuth angle of the ith blade, and $k = 1 \ldots M$ is a DOF number. The transformation assumes the blades are evenly distributed, i.e., $\phi_i = \phi_i + 2\pi(i-1)/3$, $i = 1, 2, 3$. The backward transformation, from the multiblade coordinates to the blade coordinates is given by

$$q_{i,k} = a_{0,k} + a_{1,k}\cos\phi_i + b_{1,k}\sin\phi_i\,. \tag{8.2}$$

Typically the equation of motion (EoM) is written for a mixture of blade and tower/nacelle DOFs,

$$\mathbf{M}\ddot{\mathbf{x}} + \mathbf{C}\dot{\mathbf{x}} + \mathbf{K}\mathbf{x} = \mathbf{0}, \tag{8.3}$$

with

$$\mathbf{x} = \{q_{1,1}..q_{1,M}\,, .., q_{3,1}..q_{3,M}\,, s_1..s_L\}^T, \quad \mathbf{x} \in R^{3M+L}, \tag{8.4}$$

where s_l, $l = 1..L$ are DOF measured in the non-rotating frame. For an operating wind turbine, the mass matrix $\mathbf{M}$, gyroscopic/damping matrix $\mathbf{C}$ and stiffness matrix $\mathbf{K}$ are periodic in time: $\mathbf{M}(t) = \mathbf{M}(t+T)$, $\mathbf{C}(t) = \mathbf{C}(t+T)$,

$\mathbf{K}(t) = \mathbf{K}(t+T)$, where $T = 2\pi/\Omega$ is a period of the rotor rotation and Ω is its circular frequency. Thus Eq. (8.3) describes a linear time periodic (LTP) system, and application of the classical modal approach is impossible since the basic assumption of the modal decomposition, that the system under test is linear and time invariant, is violated here.

Using Eq. (8.2) to substitute the coordinates $q_{i,k}$ into Eq. (8.4), and leaving coordinates s_l unchanged, one arrives at EoM in multiblade coordinates:

$$\mathbf{M}_B\ddot{\mathbf{z}} + \mathbf{C}_B\dot{\mathbf{z}} + \mathbf{K}_B\mathbf{z} = \mathbf{0}, \tag{8.5}$$

where

$$\mathbf{z} = \{a_{0,1}, a_{1,1}, b_{1,1} \ldots a_{0,M}, a_{1,M}, b_{1,M}, s_1..s_L\}^T, \quad \mathbf{z} \in R^{3M+L}. \tag{8.6}$$

Hansen et al. [2, 9] state that, if the rotor is isotropic, the matrices $\mathbf{M}_B$, $\mathbf{C}_B$ and $\mathbf{K}_B$ are constant, and thus MBC transformation converts the LTP system into an LTI system. Bir [8] generally disagrees with this statement but admits that, under the rotor isotropy assumption, the MBC transformation filters out all periodic terms from the EoM, except those that are integer multiples of 3 Ω. In the same paper, Bir also clarifies some typical misconceptions regarding MBC, one of them is the necessity of the stationarity of the rotor speed ($\Omega = const$).

In any event, converting the LTP system in Eq. (8.3) into the LTI system in Eq. (8.5) allows the application of the classical modal approach to the new system, i.e., presenting the system dynamics as a superposition of modes, and finding the corresponding modal parameters: modal frequencies, damping and mode shapes. This paper concerns output-only modal analysis, i.e., the operating wind turbine is loaded by pure wind and unmeasured forces due to the rotation of the turbine. Then the obtained mode shapes are transferred back to the blade coordinates using Eq. (8.2). In [4], this method was applied to simulated wind turbine data; this paper extends the analysis to the measured data and compares it with the results from another method, outlined in the next section.

When considering a time variant mechanical system, the term "mode" becomes somehow vague. If an operating wind turbine with isotropic rotor is described in multiblade coordinates, the system becomes LTI where the "modes" are well defined. Let us consider a mode of system Eq. (8.5), and assume it has the following modal parameters: the eigenvalue

$$\lambda_r = -\zeta_r\omega_r + \mathrm{j}\omega_r\sqrt{1-{\zeta_r}^2}, \tag{8.7}$$

where ζ_r represents the modal damping and ω_r is the undamped natural frequency. The corresponding mode shape is

$$\psi_r = \{a_{0,1}, a_{1,1}, b_{1,1} \ldots a_{0,M}, a_{1,M}, b_{1,M}, s_1..s_L\}_r^{\mathrm{T}}, \quad \psi_r \in C^{3M+L}. \tag{8.8}$$

The elements of the mode shape vector are complex numbers.

Employing a backward MBC transformation, it is possible to map this mode into the natural blade coordinates. For rotor angular speed Ω, the motion at the kth DOF on the ith blade corresponding to this mode will be:

$$q_{i,k}(t) = \gamma_{i,k}(t) + \alpha_{i,k}(t) + \beta_{i,k}(t), \tag{8.9}$$

where

$$\begin{aligned}
\gamma_{i,k}(t) &= e^{\mathrm{j}\omega_r t - \zeta_r\omega_r t}a_{0,k};\\
\alpha_{i,k}(t) &= \frac{1}{2}e^{\mathrm{j}(\omega_r+\Omega)t-\zeta_r\omega_r t}\,(a_{1,k} - jb_{1,k})\,e^{\mathrm{j}\frac{2\pi}{3}(i-1)};\\
\beta_{i,k}(t) &= \frac{1}{2}e^{\mathrm{j}(\omega_r-\Omega)t-\zeta_r\omega_r t}\,(a_{1,k} + jb_{1,k})\,e^{-\mathrm{j}\frac{2\pi}{3}(i-1)},
\end{aligned} \tag{8.10}$$

As one can see, in the *blade coordinates* the modes of the LTI system in Eq. (8.5) occur in groups of three, with frequencies: $\omega_r - \Omega$, ω_r, and $\omega_r + \Omega$. In general each of these modes could have a different damping ratio, ζ_r, although in Eq. (8.10). The γ component does not depend on blade's number i, meaning that all three blades oscillate in phase; this is a so-called *collective* mode. The *backward whirling* (or *anti-symmetric*) mode α has a frequency $\omega_r + \Omega$; blade number $i+1$ lags behind blade number i by $-120°$. The *forward whirling* mode β has frequency $\omega_r - \Omega$; blade number $i+1$ lags behind blade number i by $+120°$.

8.2.2 Harmonic Power Spectrum of LTP System

A single frequency input to an LTI system causes a response at the same frequency. In contrast, the same input to an LTP system, e.g., a wind turbine, causes a response that includes the excitation frequency and also an infinite number of its harmonics. An Exponentially Modulated Periodic (EMP) signal space [5] is defined to contain the frequency component at the single excitation frequency as well as its harmonics. Specifically, if the frequency of interest was ω then the EMP signal would consist of a collection of sinusoids at frequencies $\omega \pm n\Omega$, each having a different amplitude and phase. The harmonic transfer function is a matrix that relates an EMP input signal (expressed as a vector of harmonic amplitudes at $\omega \pm n\Omega$) to an EMP output signal. Details about how to derive the harmonic transfer function and then the harmonic power spectrum can be found in [10].

In practice, one would often like to express a measured signal as an EMP signal, for example in order to compute transfer functions. This is done by creating several frequency shifted copies of the signal. Specifically, suppose an output $y(t)$ is measured. An EMP output signal in the frequency domain would be expressed as,

$$\mathbf{Y}(\omega) = \left[\cdots Y_{-1}(\omega)\ Y_0(\omega)\ Y_1(\omega)\cdots\right]^{\mathrm{T}} \tag{8.11}$$

where $Y_{\boldsymbol{n}}(\omega)$ is the FFT of the nth modulated output signal $y_n(t)$,

$$y_n(t) = y(t)e^{-\mathrm{j}n\Omega t} \tag{8.12}$$

This paper primarily focuses on how to interpret the harmonic power spectrum in order to identify the natural frequencies and time periodic mode shapes of an operating wind turbine, which is modeled as an LTP system.

Previous works have shown that the harmonic power spectrum of an LTP system can be expressed in a modal summation form as,

$$S_{YY}(\omega) = E\left(\mathbf{Y}(\omega)\mathbf{Y}(\omega)^{\mathrm{H}}\right) = \sum_{r=1}^{N} \underbrace{\sum_{l=-\infty}^{\infty} \frac{\overline{\mathbf{C}}_{r,l}\mathbf{W}(\omega)_r\overline{\mathbf{C}}_{r,l}^{\mathrm{H}}}{[j\omega - (\lambda_r - \mathrm{j}l\Omega)]\,[j\omega - (\lambda_r - \mathrm{j}l\Omega)]^{\mathrm{H}}}}_{r^{\mathrm{th}}\ \mathrm{mode}} \tag{8.13}$$

where E() is the expectation and $()^{\mathrm{H}}$ is the Hermitian. $\mathbf{Y}(\omega)$ is the exponentially modulated output signal defined in Eq. (8.11). Equation (8.13) has a similar mathematical form as the power spectrum of an LTI system,

$$S_{YY}(\omega) = \mathrm{E}\left(Y(\omega)Y(\omega)^{\mathrm{H}}\right) = \sum_{r=1}^{N} \frac{\psi_r S_{UU}(\omega)\psi_r{}^{\mathrm{H}}}{[\mathrm{j}\omega - \lambda_r]\,[\mathrm{j}\omega - \lambda_r]^{\mathrm{H}}} \tag{8.14}$$

where $Y(\omega)$ is the spectrum of measured output for the LTI system. The numerator in Eq. (8.13) contains $\mathbf{W}(\omega)_r$, which is the auto-spectrum of the net force exciting the rth mode of the time periodic system. This is similar to the input autospectrum, $S_{UU}(\omega)$ in Eq. (8.14), which reduces to an identity matrix when the structure is excited with uncorrelated white noise.

However, there are also two notable differences between the harmonic power spectrum in Eq. (8.13) and the conventional power spectrum in Eq. (8.14). First, the harmonic power spectrum not only contains a summation over the modes, whose eigenvalues are λ_r, but each mode also appears at several harmonics $\omega_r - l\Omega$. Hence, the harmonic power spectrum has peaks near each natural frequency ω_r, and also at the frequencies $\omega_r - l\Omega$ for any integer l. Second, the mode vector $\overline{\mathbf{C}}_{r,l}$ in the harmonic power spectrum is no longer a collection of vibration amplitudes at different measurement locations (note the definition of mode in Sect. 8.2.1), as ψ_r in Eq. (8.14). Instead, $\overline{\mathbf{C}}_{r,l}$ consists of the Fourier coefficients that describe the rth time periodic mode shape collected into a vector as,

$$\overline{\mathbf{C}}_{r,l} = \left[\cdots C_{r,-1-l}\ C_{r,-l}\ C_{r,1-l}\cdots\right]^{T}$$

$$C(t)\psi_r(t) = \sum_{l=-\infty}^{\infty} C_{r,l}e^{\mathrm{j}l\Omega t} \tag{8.15}$$

$C(t)$ is the output vector in the state space model of the equation of the motion [11], indicating which DOF is being measured. For the wind turbine measurement using accelerometers, $C(t)$ is simply a one at each senor location. Theoretically, a periodic mode shape $\psi_r(t)$ should be described with a Fourier series of infinite order, yet one would expect that most systems can be well approximated with a finite, perhaps even small number.

The harmonic power spectrum is estimated in a conventional manner. Assuming $n = -p \ldots p$ is used to modulate the acquired output, the modulated signal forms a matrix of $2p + 1$ copies of the signal at a certain number of frequency lines. The harmonic power spectrum then has a dimension of $(2p + 1) \times (2p + 1)$ by the number of frequency lines. Since each column (or row) in the harmonic power spectrum contains similar information about the LTP system, only the primary column (center column) is used in the identification. The procedure of identifying time periodic modes from the harmonic power spectrum can be summarized as,

1. Record the response $y(t)$ at any sensor on the wind turbine under random excitation.
2. Construct the exponentially modulated periodic output signals in the time domain using $y_n(t) = y(t)e^{-\mathrm{j}n\Omega t}$, with $n = -p \ldots p$
3. Split the modulated output signals into many sub-blocks with the desired level of overlap. Apply a Hanning window to each block and compute the spectra of modulated output signals, $Y_n(\omega)$
4. Compute the primary column of the harmonic power spectrum with $S_{\mathbf{YY}}(\omega)_{n,0} = \mathrm{E}(\mathbf{Y}(\omega)Y_0(\omega)^{\mathrm{H}})$ where the expectation operator denotes the average over all of the sub-blocks.
5. Use peak-picking or curve-fitting routines to identify the rth natural frequency ω_r and the mode vectors $\overline{\mathbf{C}}_{r,l}$ at different harmonics.
6. Align $\overline{\mathbf{C}}_{r,l}$ for various l to compare different estimates of the same mode vector using Eq. (8.15). Apply singular value decomposition to find the best estimate from all Fourier coefficient vectors [7].
7. Use Eq. (8.15) to reconstruct the time periodic mode shape $\psi_r(t)$.

8.3 Experimental Setup

This paper applies the two methods described in the previous section to operational measurements from a Vestas V27 wind turbine. The Vestas V27 is a 225 kW medium size upwind pitch regulated wind turbine (Fig. 8.1a). An extensive measurement campaign took place from October 2012 through May 2013. Each blade of the wind turbine was instrumented with 12 accelerometers (Bruel and Kjaer Type 4507 and 4508), including ten accelerometers in the flapwise direction (five on the leading edge and five on the trailing edge) and two accelerometers in the edgewise direction (Fig. 8.1b). Since the MBC-based method requires symmetry of the measurement system, special care was taken to mount the sensors on all three blades as similar to each other as possible, both location- and direction-wise. The nacelle was instrumented with three triaxial accelerometers (Fig. 8.1c). In order to estimate the instantaneous rotor position (azimuth) and rotor angular speed, two DC accelerometers, attached to the rotor's hub, were employed. To improve the estimate of the azimuth angle, a tachoprobe was also installed on the wind turbine's High-Speed Shaft (the HSS, connects the gearbox to the electrical generator). A pitch sensor was installed inside the hub; its readings were used for selecting recordings with no or relatively small pitch activity. In addition, two IRIG-B signals were used to synchronize the signals from the rotor and nacelle sensors. In total, 40 channels were recorded using B&K LAN-Xi data acquisition modules located in the hub and wirelessly transferred to the nacelle, where another 11 channels were measured. All channels were recorded synchronously at a sampling frequency of 4,096 Hz. Additional details regarding the measurement setup can be found in [3].

As described previously, the operating wind turbine is modeled as an LTP system. This modeling assumes constant rotor speed during the observation period. Unfortunately, the rotating speed is rarely constant in practice. Figure 8.2 shows a 5 min portion of the time history of the rotating speed computed from one of the DC accelerometers. The rotating frequency varies from 0.527 to 0.543 Hz over this time interval. Therefore, the first step was to select the datasets where the rotating speed is the steadiest. Furthermore, any pitch activity changes the in-plane and out-of-plane stiffness of the blade. Thus the second criterion was to select the datasets with minimum pitch activity. This was done using filtering and sorting options of the recording database. Eventually, the data taken at December 16, 2012 was selected (20 min long). The rotating speed, pitch angle and wind speed (30 m above the ground) for this data set are listed in Table 8.1.

The correct azimuth angle is a key parameter for both MBC and harmonic power spectra based methods. A lot of attention was paid to derive the azimuth angle from the readings of three redundant sensors: two DC accelerometers located in the hub and the tachoprobe measuring HSS angular speed (the exact gear ratio is around 23.3333). It was found that the tachoprobe provided the most accurate measurement of the rotating frequency. The average rotating frequency over this 20 min measurement was 0.5369 Hz with a standard deviation of 0.0007 Hz. This average rotating frequency was then used to compute the azimuth angle of each blade.

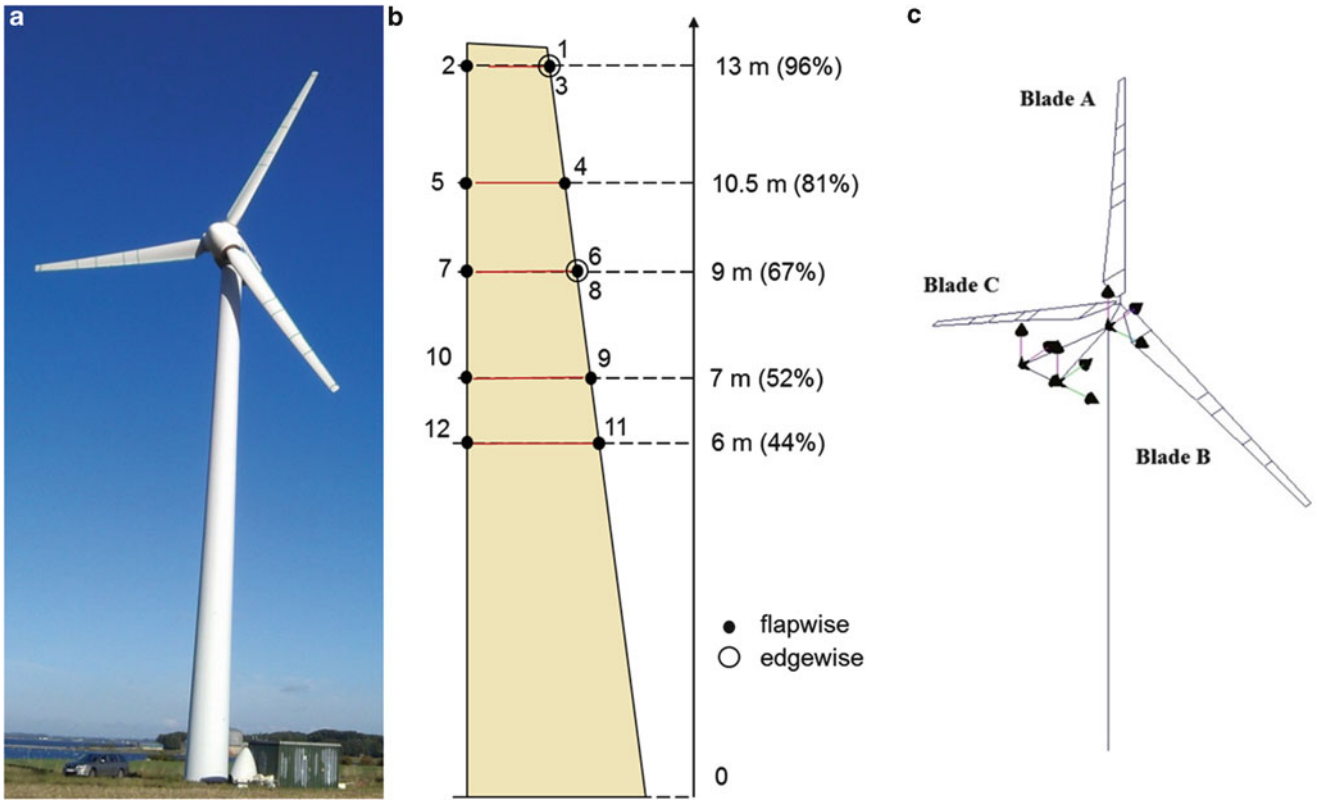

Fig. 8.1 (**a**) Vestas V27 with blades instrumented with accelerometers. (**b**) Location and orientation of the accelerometers on the blades. (**c**) Location of triaxial accelerometers in the nacelle

Fig. 8.2 Time history of rotating frequency

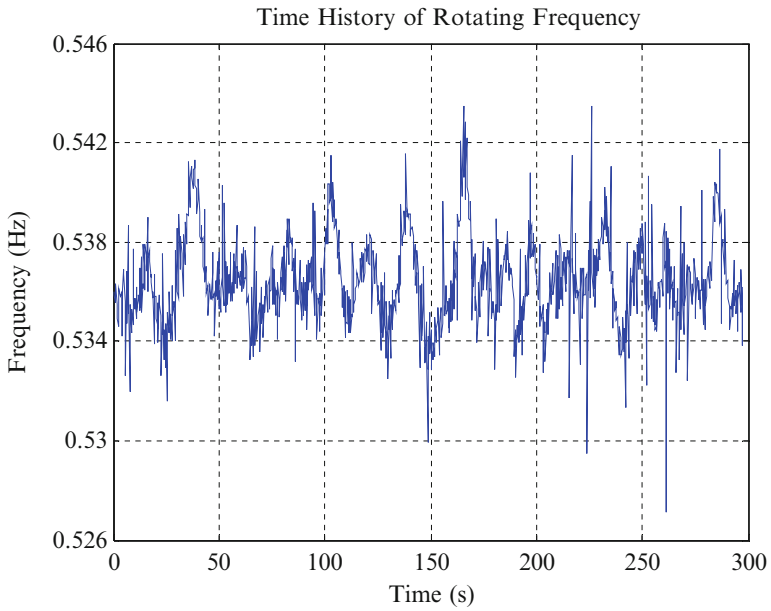

Table 8.1 Test conditions for the selected dataset

	DC1 (Hz)	DC2 (Hz)	Tacho (Hz)	Pitch angle (°)	Wind speed (m/s)
Mean	0.5370	0.5370	0.5369	−0.2150	4.7300
Maximum	0.5536	0.5548	0.5385	−0.0525	6.6850
Minimum	0.5228	0.5159	0.5352	−0.4925	2.6250
Standard deviation	0.0064	0.0074	0.0007	0.0850	0.6710

8.4 Preliminary Analysis

This section describes a preliminary analysis of the measured data, which can be conducted before stepping into the more complex modeling techniques. For the preliminary analysis, four sensors were selected, see Table 8.2. These sensors were located on the trailing edge at the tip, and at 9 m from the root of the blade.

First, the power density spectra (PSD) of the signals was calculated ($\Delta f = 1.125 \times 10^{-2}$ Hz; block size 89 s; 67 % overlap; Hanning window; 38 averages); the PSD of the tip acceleration signals averaged over 20 min of observation time, are shown in Fig. 8.3.

Analyzing Fig. 8.3, one can observe:

1. The level of the flapwise vibrations is higher than the level of edgewise vibrations;
2. At low frequencies, the response in both flapwise and edgewise directions is heavily dominated by harmonics. Two families of the harmonics can be identified: the first are the harmonics of the rotor (shown by the blue vertical lines in Fig. 8.3), the second family is due to the HSS fundamental frequency at 12.52 Hz modulated by the rotor frequency (the red vertical lines in Fig. 8.3);
3. The effect of the "fat tails" mentioned in [12] can be clearly seen on the lowest rotor harmonics. The higher harmonic peaks (starting from the fifth rotor harmonic) become narrower, and eventually have the appearance of typical harmonic peaks.
4. Flapwise vibrations are less contaminated by the rotor and gearbox harmonics at higher frequencies;
5. The readings of the accelerometers located in the same positions on different blades are not identical, which is either due to imprecise mounting or different dynamic characteristics of the blades (which is possible since one of the blade of this particular wind turbine was replaced some years ago). Since the MBC transformation assumes rotor isotropy and symmetry of the observation system, this could be a serious obstacle for the application of the MBC-based method. In contrast, the harmonic power spectrum method does not require these assumptions.
6. Note the double peak at approximately 3.5 Hz on the edgewise signal spectra (see the inset): one may expect a double peak (since the frequencies of the two anti-symmetric modes may slightly differ) but it is not normal that the higher frequency peak and the lower frequency peak dominate at different blades. If the rotor was isotropic, the shape of the spectra averaged over many rotor revolutions is expected to be the same for all three blades. Therefore this observation rather speaks for the rotor anisotropy than for the imperfection of the sensors mounting.

Table 8.2 Acceleration signals selected for analysis

Name (Fig. 8.1b)	Description
1f	Tip, trailing edge, flapwise direction
3e	Tip, trailing edge, edgewise direction
6f	9 m from the root, trailing edge, flapwise
8e	9 m from the root, trailing edge, edgewise direction

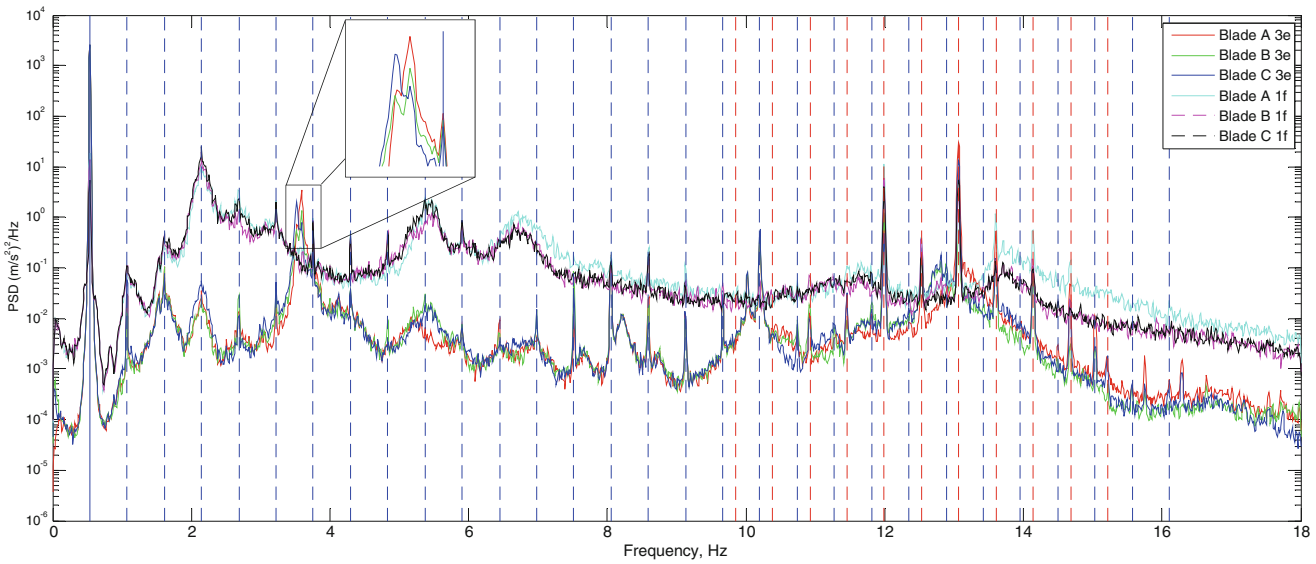

Fig. 8.3 PSD of the tip acceleration signals. *Blue dash line*—rotor fundamental, *blue dotted lines*—rotor harmonics, *red dashed line*—high speed shaft fundamental, *red dotted lines*—its sidebands

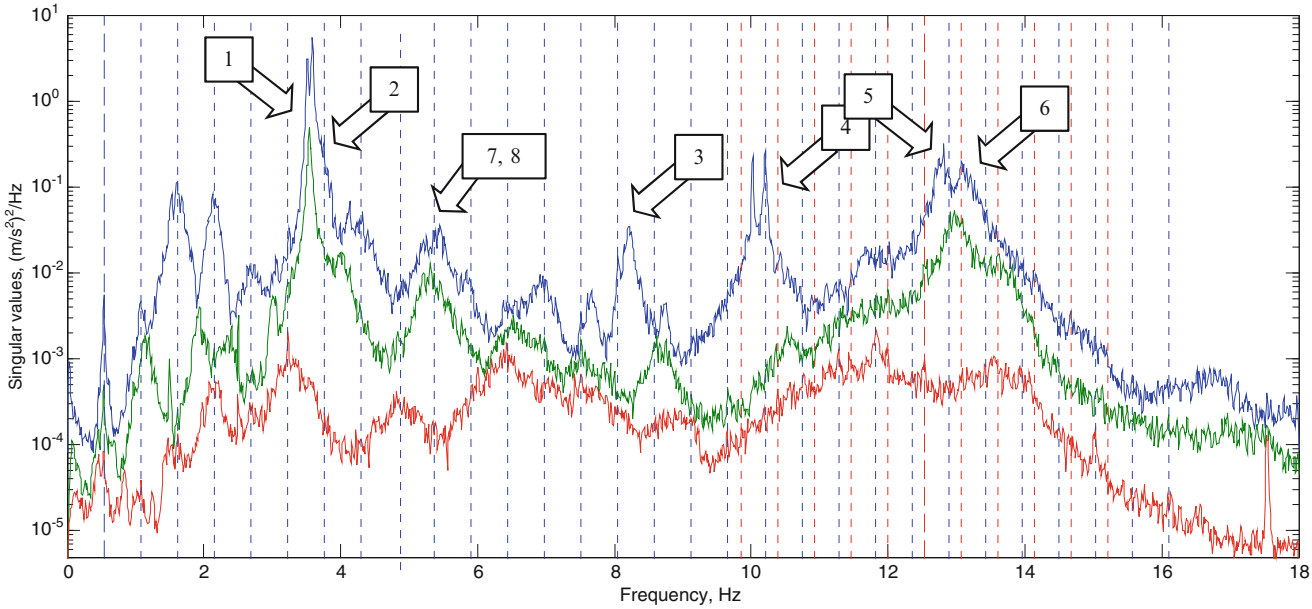

Fig. 8.4 Singular values of the cross-spectra matrices calculated for sensors 3e on all three blades

Since the harmonics are undesirable in further analysis, the time-synchronous averaging (TSA) algorithm was employed to remove the harmonics. TSA was applied in two runs, first removing the rotor harmonics, and second—the sidebands of the HSS fundamental frequency. The tacho events are generated from the instantaneous rotor azimuth $\phi_1(t)$, which is estimated as explained in Sect. 8.3. The detailed explanation of the TSA method can be found in [13]. Due to the "fat tails" phenomena, TSA does not significantly affect the lowest rotor harmonics but effectively removes the higher harmonics and HSS sidebands.

Along with the PSD, the singular value decomposition (SVD) can shed some light on how many independent vectors should be used to describe system behavior at different frequencies. The SVD was performed on the 3×3 cross-spectra matrix computed between the sensors located at the same point on all three blades. Figure 8.4 shows the three singular values computed for the signal 3e after the harmonics were removed by TSA.

If focusing on the edgewise vibrations, SVD reveals some expected modal behavior, for example, arrows #1, 2 and #5, 6 in Fig. 8.4 denote the two edgewise anti-symmetric modes, #3,#4 are perhaps the edgewise collective modes, #7, 8 are the traces of the two flapwise anti-symmetric modes, which also have an edgewise component. However, at this point this is just a guess-work; the modal analysis shall reveal the true dynamics of the wind turbine.

The next step will be to apply the MBC transformation to the data according to Eq. (8.1). The instantaneous rotor azimuth $\phi_1(t)$, which participates in Eq. (8.1) is estimated as explained in Sect. 8.3. The geometrical interpretation of multiblade coordinates can be found in [14]. The spectra of the multiblade coordinates a_0, a_1 and b_1 are shown in Fig. 8.5.

Analyzing Fig. 8.5, one can observe the following:

1. The peak at 1 Ω (rotor fundamental) has almost disappeared, while the peak at 3 Ω (3rd harmonic, the so-called *blade passing frequency*) has increased. This agrees with Bir's statement that MBC transformation can be considered as a filter stopping all harmonics except those that are integer multiples of 3 Ω [8].
2. The anti-symmetric coordinates a_1 and b_1 (green and blue curves respectively) follow each other closely, in contrast the symmetric (collective) coordinate a_0 (red curve) is quite distinct. Thus MBC effectively separated collective blade behavior from the anti-symmetric.
3. There are two types of behavior of the peaks identified in the blade spectra (Fig. 8.4): some peaks like peaks #1, 2 become two well separated peaks #A, B while the other peaks like #4 keep their location (peak #C). The first type of peaks is typical for anti-symmetric (or whirling) modes, while the second type—for collective modes. In blade coordinates, the whirling modes are often very close in frequencies (e.g. peak pair #1, 2 and pair #5, 6 in Fig. 8.4). In multi-blade coordinates, these peaks are typically separated: (peak pair #1, 2 becomes #A, B and pair #5, 6 becomes #D, E). The distance between the new peaks in the pairs is about 2 Ω.

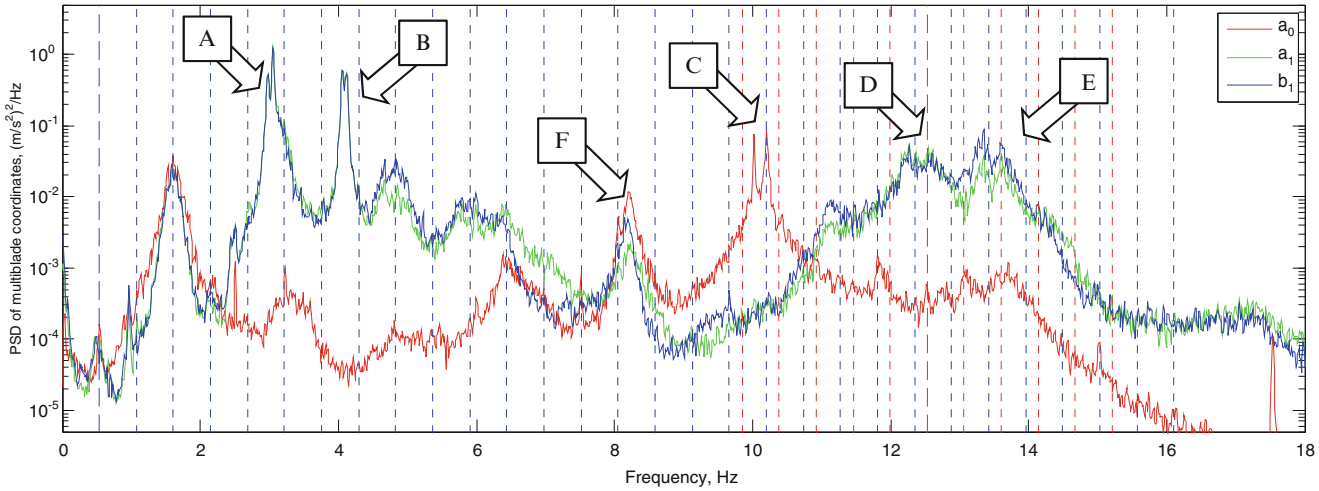

Fig. 8.5 PSD of multiblade coordinates for 3e sensor location

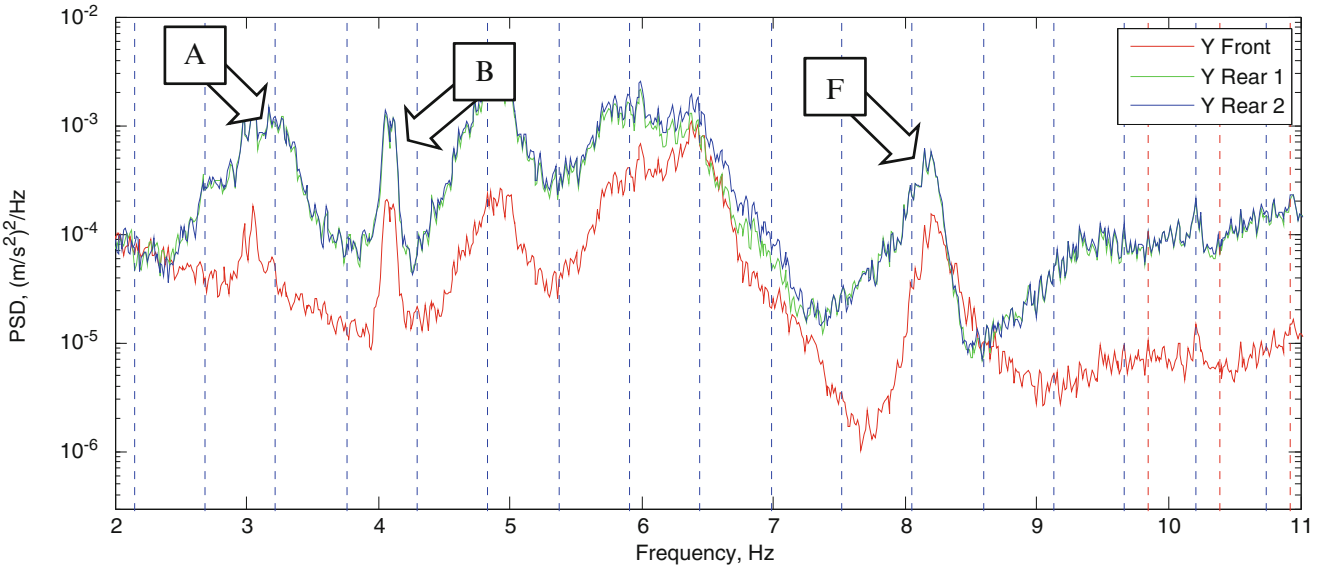

Fig. 8.6 PSD of the nacelle acceleration signals, side-to-side direction: *red*—front, *green*—rear right, *blue*—rear left. The *letters* denoting the peaks are the same as in Fig. 8.5

It is also important to note that the peaks seen on the MBC coordinates (Fig. 8.5) can also be traced in the nacelle acceleration spectra (Fig. 8.6). This makes it possible to identify many rotor modes using only tower and nacelle data, was reported in [15].

8.5 Modal Analysis of Operational Turbine using Multiblade Coordinate Transformation

The analysis performed so far is purely signal processing, with no modeling introduced and no assumptions made. In the following sections, we assume that the structure under test is LTP, and will model its dynamics via modal decomposition.

In this section we perform operational modal analysis (OMA) on the experimentally obtained data pre-processed by harmonic removal and multiblade coordinate transformation, as detailed in Sect. 8.4. The new time histories become the input to OMA. As will be explained later, the main focus is placed on the edgewise motion, since it has more interesting time-periodic behavior.

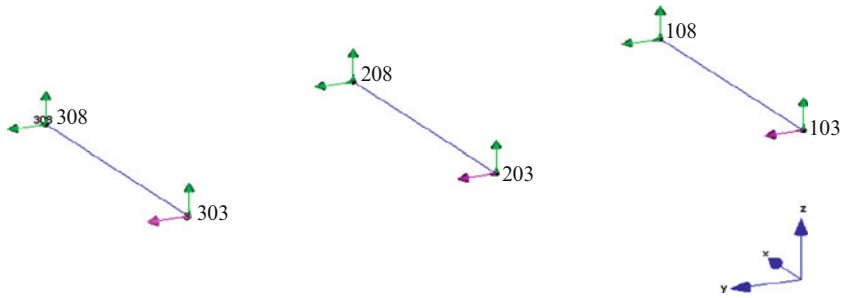

Fig. 8.7 Simple geometry indicating 6 multiblade coordinates

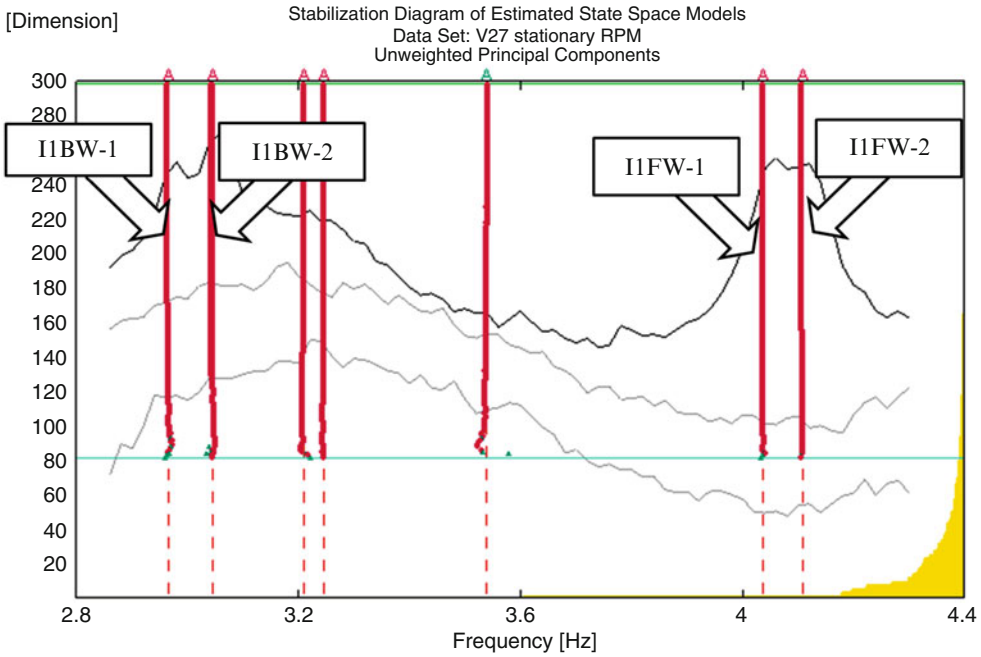

Fig. 8.8 Stabilization diagram around first in-plane modes

Table 8.3 Modal parameters of the mode shown in Fig. 8.8

Mode	Frequency (Hz)	Damping ratio (%)	Notes	(Average) phase difference between a_1 and b_1 (at the tip)
I1BW-1	2.97	2.8	$3.51 - \Omega$	$-86.1°$
I1BW-2	3.05	1.8	$3.58 - \Omega$	$-87.4°$
I1FW-1	4.04	1.1	$3.51 + \Omega$	$85.2°$
I1FW-2	4.11	0.8	$3.58 + \Omega$	$90.2°$

The OMA stochastic subspace identification (SSI) algorithm (Bruel and Kjaer Type 7760) was used for identification. Twelve channels [3× (1f, 3e, 6f, 8e, Fig. 8.1b)] were selected for the analysis. The data were decimated ten times; thus the new sampling rate is 40.96 Hz.

Typically, modal analysis software uses test object geometry in order to visualize measured DOFs and to animate the modes. In the case of multiblade coordinates such visualization is not physical; however it is found very useful in order to give mode nomenclature. Figure 8.7 shows the simple geometry used for the visualization. DOFs 10* denote multiblade coordinate a_0, 20* are a_1 and 30* are b_1. Points *03 correspond to the blade tip, and ones *08—to the middle of the blade. Z-direction corresponds to flapwise DOFs, and Y—to edgewise direction. If, when animating the mode, a_0 dominates, this is a collective mode. Dominating a_1 and b_1 indicate anti-symmetric (whirling) modes. If the phase between a_1 and b_1 is $-90°$, this is a backward whirling mode; the phase of $+90°$ indicates the forward whirling. If DOFs *03 and *08 move in-phase, this is a first bending mode, while anti-phase points to the second bending mode. Identification of higher modes is restricted by the low spatial resolution, especially in the edgewise direction.

Figure 8.8 shows the stabilization diagram in the range 2.8–4.4 Hz corresponding to peaks #A, B in Fig. 8.6; the corresponding mode table is shown below. SSI algorithm finds four edgewise modes, shown in the table (Table 8.3), the other modes are flapwise dominated or noise modes, which are not considered here. The modes I1BW-1 and I1FW-1 (abbreviations

Table 8.4 Multiblade coordinates dependence on phase ϕ

ϕ	a_0	a_1	b_1	Phase between a_1 and b_1	Mode name
0	$A\sin(\omega t)$	0	0	Not defined	Collective
$+120°$	0	$A\sin((\omega+\Omega)t)$	$-A\cos((\omega+\Omega)t)$	$+90°$	Forward whirling
$-120°$	0	$A\sin((\omega-\Omega)t)$	$A\cos((\omega-\Omega)t)$	$-90°$	Backward whirling

for in-plane 1st bending, back- or forward whirling respectively) are both originated from the peak at 3.51 Hz on the edgewise signals spectra; the frequencies of these modes are $3.51 \mp \Omega$ respectively. The modes I1BW-2 and I1FW-2 are originated from the peak at 3.58 Hz, and their frequencies are $3.58 \mp \Omega$. The presence of the four modes found by OMA-SSI in multiblade coordinate data is *an indication of rotor anisotropy*; these modes are not physical, this is an artifact due to the violation of the rotor isotropy assumption.

Indeed, if the rotor was isotropic, the (averaged) spectra of the accelerations measured on all three blades should have almost identical magnitude, and the phase between the signals measured on the neighboring blades should be equal and their sum should be $0 \pm 360°$: $\phi_{AB} = \phi_{BC} = \phi_{CA} = \phi$ and $\phi_{AB} + \phi_{BC} + \phi_{CA} = 0 \pm 360°$. This is only possible if the phase is either 0° (for collective behavior) or ±120° ("+" for forward whirling and "−" for backward whirling). Suppose the vibrations of the ith blade have a peak at a certain frequency ω: $q_i = A\sin(\omega t - \phi\ (i-1))$. Depending on the phase ϕ, after the MBC transformation in Eq. (8.1), one obtains the multiblade coordinates according to Table 8.4.

This means that in the case of the isotropic rotor, a peak in the blade vibration spectra should become one peak in the multiblade coordinate spectra, not two, as we experienced here. Only one mode would then be found at that peak (in MBCs) but here two modes have erroneously been extracted. Here, we observe two closely spaced peaks in the blade spectra around 3.5 Hz (Fig. 8.3) which presumably correspond to backward and forward whirling modes; let's denote the frequencies of the peaks by ω_{BW} and ω_{FW} respectively. If the rotor was isotropic, the spectral magnitudes of all three blades would be approximately the same, and the phase would be $-120°$ at ω_{BW} and $+120°$ at ω_{FW}. After MBC transformation, we would discover two peaks in the MBC spectra: the backward whirling mode at $\omega_{\mathrm{BW,MBC}} = \omega_{\mathrm{BW}} - \Omega$ and forward whirling at $\omega_{\mathrm{FW,MBC}} = \omega_{\mathrm{FW}} + \Omega$, and these modes would then correspond to the backward and forward whirling modes of the MBC system.

Unfortunately, in the case of the anisotropic rotor, this analysis does not bring such clear results. Applying MBC transformation here, we found four modes at $\omega_{\mathrm{BW}} - \Omega$, $\omega_{\mathrm{BW}} + \Omega$, $\omega_{\mathrm{FW}} + \Omega$ and $\omega_{\mathrm{FW}} - \Omega$, as it is seen in Fig. 8.8. Thus, one can conclude that use of the MBC transformation cannot be recommended in the case of anisotropic rotors. Instead, we will recommend the Harmonic Power Spectrum method demonstrated below.

8.6 Modal Analysis of Operational Turbine using the Harmonic Power Spectrum Method

The turbine rotated at an average speed of 0.5369 Hz. The measured response of the blades in the edgewise direction on all three blades (in-plane sensors 3e and 8e) as well as the response on the front of the nacelle in the lateral and vertical directions were collected into a response vector with eight outputs. This response was then exponentially modulated with $n = -4 \ldots 4$ according to step 2 in Sect. 8.2.2, using the response at the tips of the three blades as references. Then, the modulated signals were split into 73 sub-blocks with a block size of 119 s (64 revolutions) and 88 % overlap. A Hanning window was applied to reduce the leakage. The resulting harmonic power spectrum matrix had 72 outputs (8 points and 9 harmonics for each) by 3 references. The complex mode indicator function (CMIF) of this HPSD matrix was then found and is shown in Fig. 8.9. Similar to that in preliminary analysis, the rotor harmonics and a cluster of sideband harmonics around 12.52 Hz due to the HSS dominate the response. Observing more closely, one can see another cluster of peaks centered around 3.59 Hz with several strong sideband harmonics, each separated with the rotating frequency. Those peaks are evidence of linear time periodic behavior and will be the focus of the following analysis.

Figure 8.10 shows an expanded view of the spectrum near 3.5 Hz, where the first edgewise modes of the blades are most active. The spectrum clearly shows two peaks near 3.5 Hz and the shape of the first (blue) and second (green) singular value curves strongly suggests that two modes are present at that peak. Several modulations of the peak are also seen near 3.0, 4.0 and 4.5 Hz. The full harmonic power spectrum matrix was curve fit using a variant of the AMI algorithm [16, 17], focusing only on the peaks near 3.5 Hz. Two modes were identified with natural frequencies 3.5184 and 3.5867 Hz and damping ratios 0.00569 and 0.00355. The mode vectors for each mode are vectors of Fourier coefficients which describe the motion of the mode at the natural frequency, plus motion at nine harmonics of the natural frequency for $n = -4 \ldots 4$. This is summarized in Fig. 8.11, which shows the magnitude and phase of the response at several points on the turbine for each harmonic of each

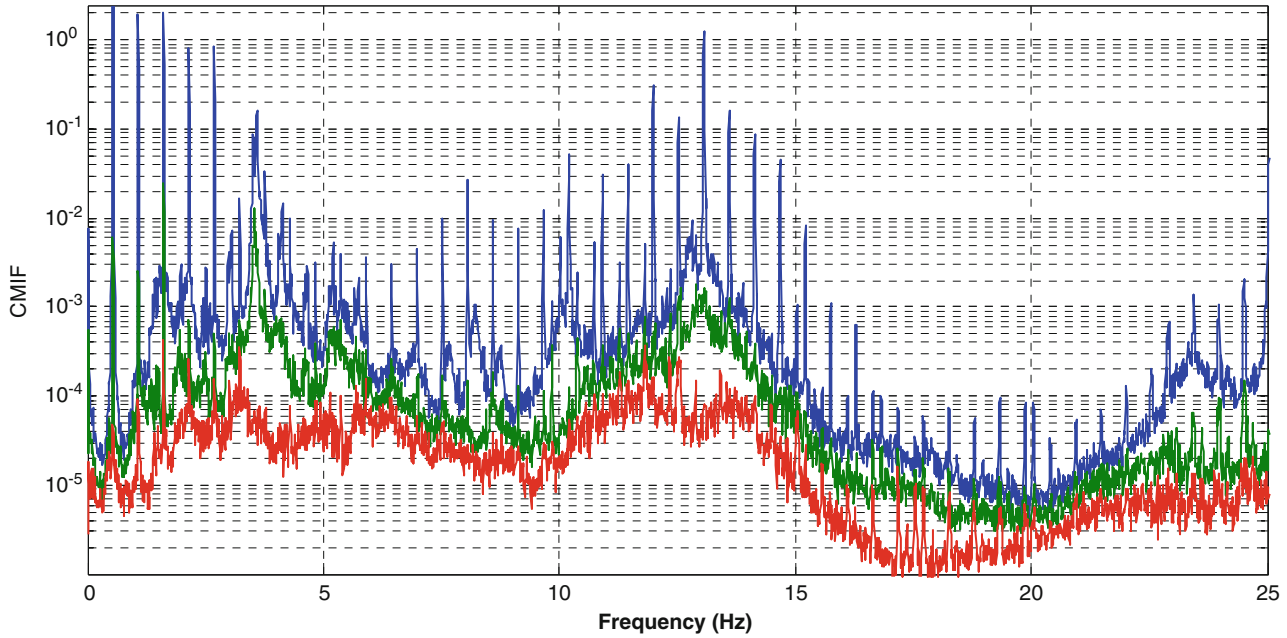

Fig. 8.9 Complex mode indicator function of the harmonic power spectrum matrix for the eight edgewise sensors using the edgewise response at the blade tips as references

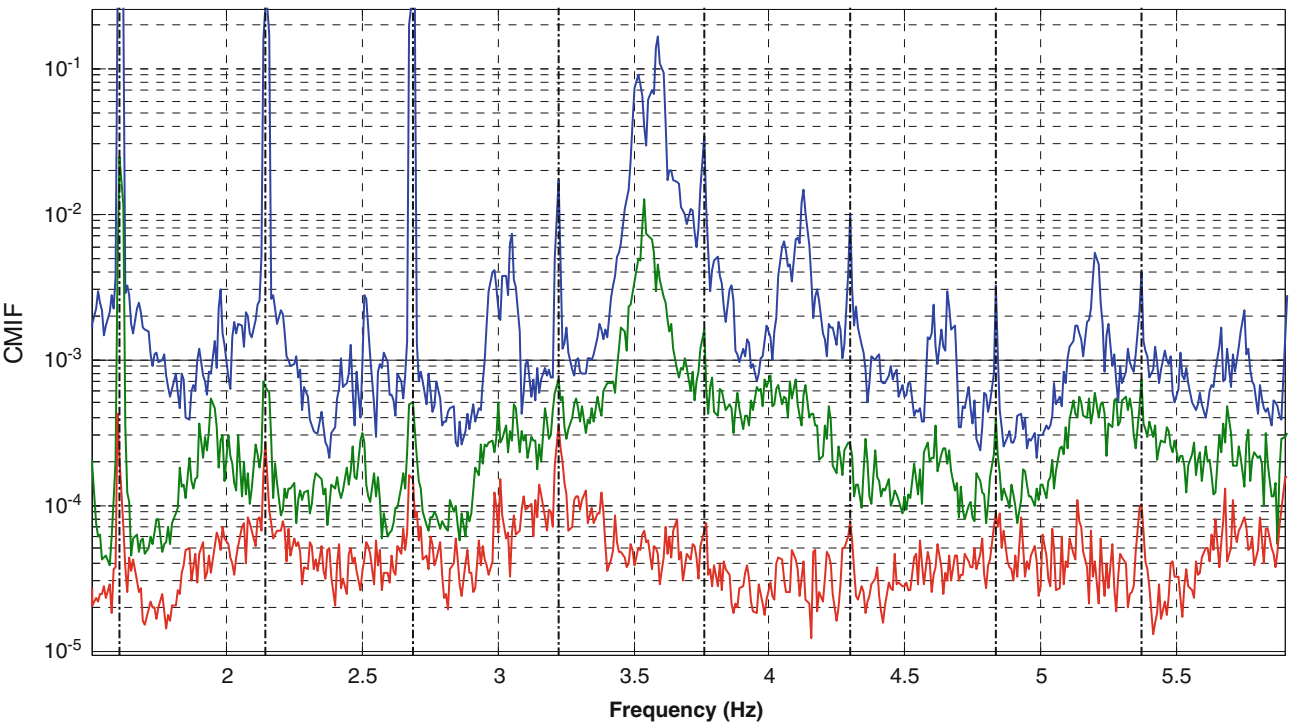

Fig. 8.10 Zoom in on harmonic power spectrum in Fig. 8.9

of these modes. As the motion is quite a bit more complicated than for an LTI system, some care will be taken to explain the meaning of this result.

First consider the mode at 3.518 Hz. The mode shape in Fig. 8.11 shows that the motion of the blades is dominated by motion at the 0th harmonic, or 3.518 Hz. Blade A moves about 180° out of phase with blades B and C. On the other hand, the tower motion is predominantly at the −1 and 1 harmonics, or 2.982 and 4.055 Hz. This was evident in Fig. 8.6 which showed the spectrum of the motion of the nacelle. The blades also exhibit some vibration at these frequencies, although at

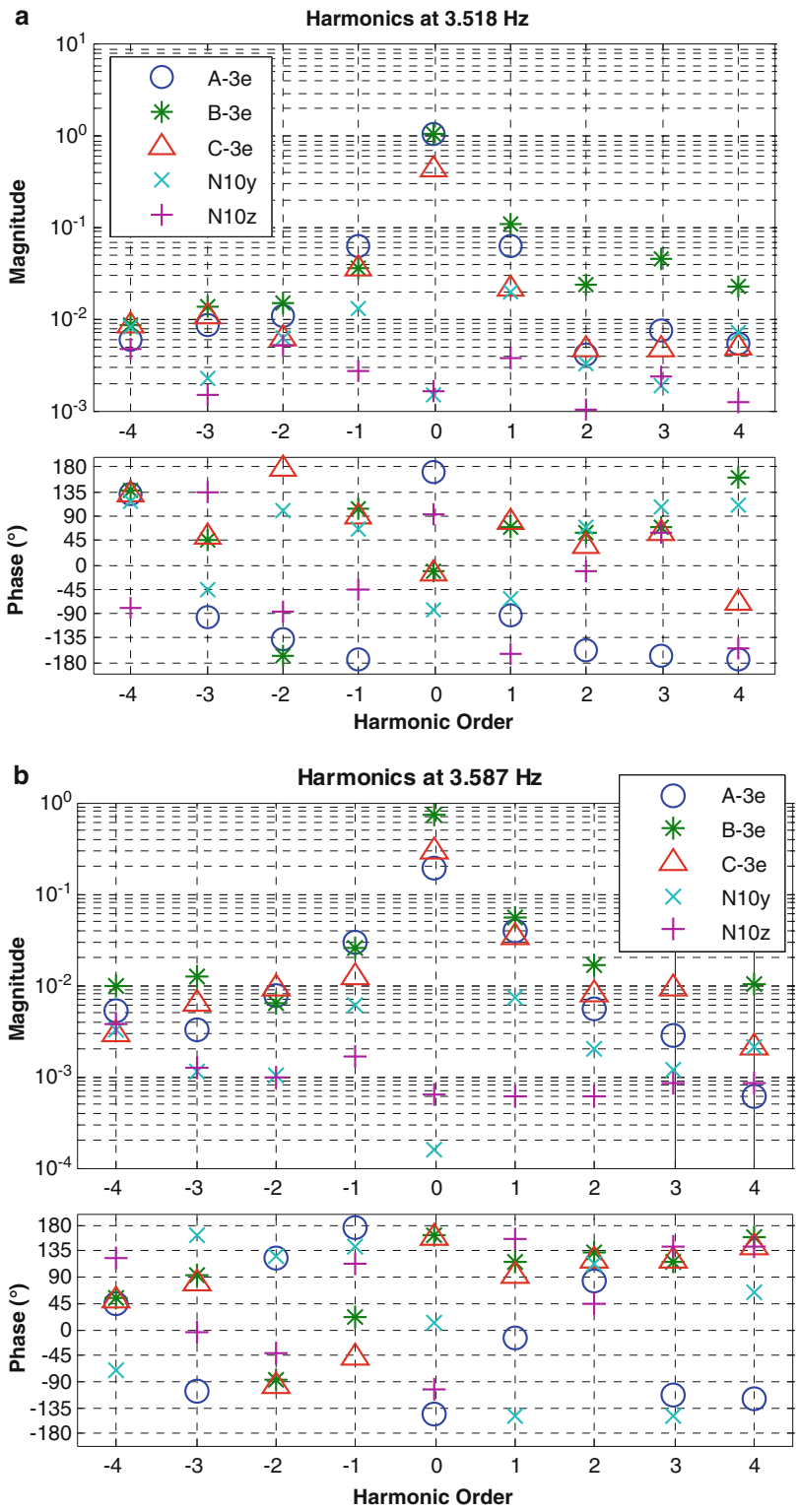

Fig. 8.11 Identified Fourier coefficients on all the blades plotted against harmonic order. (**a**) Harmonic at 3.52 Hz, (**b**) harmonic at 3.59 Hz

4.055 Hz it is about an order of magnitude smaller than the dominant motion and at 2.982 Hz it is smaller still. The higher harmonics ($|n| > 1$) are quite small and so their validity is questionable.

The mode at 3.587 Hz behaves in a similar manner, with the dominant motion being at the 0th harmonic and with relatively weak higher harmonics. The motion of the tower is also considerably smaller in this mode. In this mode blade A is about 45° out of phase with the other two blades and blade B has significantly higher amplitude than the other blades. It is interesting to

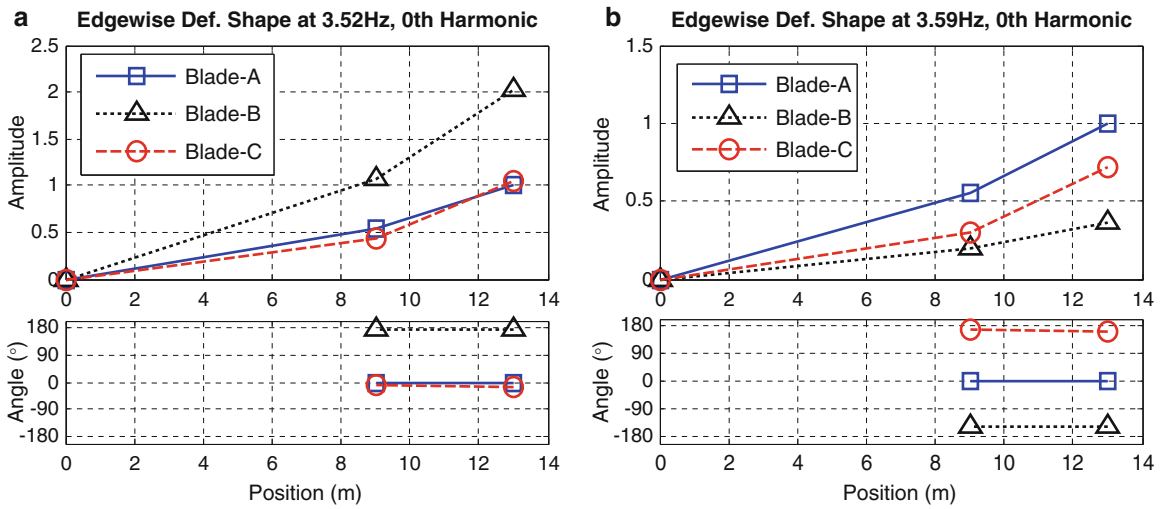

Fig. 8.12 Deformation shape identified by AMI in 0th harmonic (**a**) at 3.518 Hz, (**b**) at 3.587 Hz

note that these two modes do follow the expected trends for the edgewise modes of an isotropic wind turbine. As illustrated in [6, 9] and discussed in the previous section, a wind turbine typically exhibits backward and forward whirling modes, which in the tower reference frame (or in MBCs) occur at the tower vibration frequencies, or 2.982 and 4.055 Hz in this case. In the blade reference frame these modes would be closely spaced, and occur approximately equidistant between the two frequencies observed in the tower. While these modes are typically closely spaced (even repeated for an isotropic turbine, see e.g. [9]) they can be distinguished by the phase of the motion of the blades as discussed previously. The LTP modes identified for these two edgewise modes do not seem to follow the expected trends, but fortunately the motion observed is readily described by a linear time periodic model; the identified time-periodic shapes could be used to predict the motion of the structure or to validate a model that included the anisotropy of the turbine.

Figure 8.12 shows the deformation pattern that the structure would experience as a result of only the 0th harmonics at 3.518 and 3.587 Hz. Since the motion of the blades is dominated by the 0th harmonic, one can imagine the blades deforming into this shape and while simultaneously oscillating with perturbations about 10 % as large as these at the -1 and $+1$ harmonics. (These deformation shapes are also precisely what one would obtain if a conventional output-only modal analysis were performed.) The vibration amplitude at the hub (Position $= 0$ m) is shown as zero to aid in visualizing the blade motion. The blades clearly have different amplitudes in each mode, yet the two sensors on each blade move precisely at the same phase and the deformation shapes are as one might expect for a first bending mode of a cantilever beam. Figure 8.13 shows the motion of the blades in the 1st harmonic in a similar format. It is interesting that these harmonics also show about the same phase across the sensors on each blade, yet these shapes are different than those at the 0th harmonic. The net effect of these harmonics would be to cause the total deformation of the blades to change somewhat from blade to blade over each 3.52 or 3.59 Hz cycle.

8.7 Conclusion

An operating wind turbine has to be modeled as an LTP system to correctly characterize its time periodic behavior. In this work, two methods suitable for LTP systems, namely, the multiblade coordinate transformation and the harmonic power spectrum, were employed to identify the modes of an operating wind turbine. The vibration data were obtained from an operating Vestas V27 wind turbine instrumented with accelerometers on the blades and the nacelle.

From the accelerometer readings, it was observed that the wind turbine rotor is anisotropic; therefore the MBC transformation will fail to convert the LTP system into an LTI system. It was shown that application of the MBC transformation lead to erroneous results. In contrast, the harmonic power spectrum does not require the rotor to be isotropic. The method was successfully applied; for demonstration purposes, and two edgewise (in-plane) bending modes were identified and analyzed in detail. In this particular case, the experimental data revealed that the magnitude of the sideband harmonics in the blade reference frame was an order of magnitude lower than the central frequency component. If these sidebands were negligible then one could use straightforward operational modal analysis on the data. However, then one is

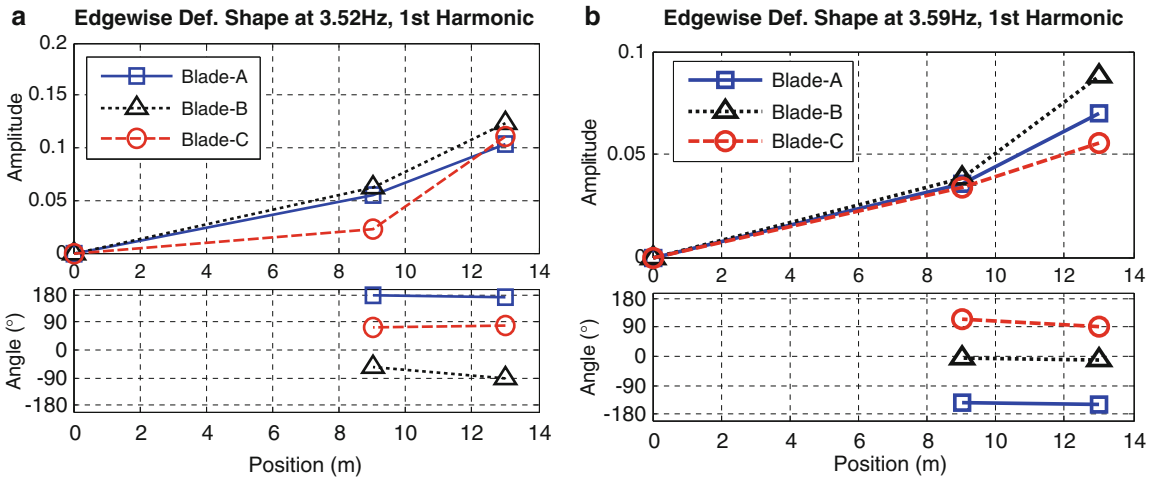

Fig. 8.13 Deformation shape identified by AMI in 1st harmonic for modes centered at (**a**) at 3.518 Hz, (**b**) at 3.587 Hz

faced with a dilemma because the same modes appear at different frequencies in the tower measurements. In any event, the harmonic spectrum method allows on to easily identify the harmonic content in each mode and to robustly determine the number of modes present in the data.

Comparing the two methods in application to experimental modal analysis of operating wind turbine, the harmonic power spectrum method is strongly recommended for most cases. Firstly, since the rotor isotropy is not initially known, using of MBC transformation may result in an erroneous modal identification. Secondly, the MBC method requires instrumentation of all three blades and, besides this, a precise symmetric mounting of accelerometers on the blades. If the sensors on one blade should fail then the method cannot be used. The harmonic power spectrum method does not require this, which makes it is much more practical in a real life situation. The harmonic power spectrum directly identifies the natural frequencies, damping ratios and the periodically time-varying modes that describe the motion of the blades in the rotating frame and the motion of the tower in the fixed frame. These modal parameters can be compared with the analytically derived modes of the turbine, obtained through a Floquet analysis, to validate an anisotropic model for the turbine. The methods will be further compared and these ideas will be further developed in the next stage of the work.

References

1. Coleman RP (1943) Theory of self-excited mechanical oscillations of hinged rotor blades. Langley Research Center. http://ntrs.nasa.gov/
2. Hansen MH (2003) Improved modal dynamics of wind turbines to avoid stall-induced vibrations. Wind Energy 6:179–195
3. Tcherniak D, Larsen GC (2013) Applications of OMA to an operating wind turbine: now including vibration data from the blades. Presented at the 5th international operational modal analysis conference, Guimarães
4. Tcherniak D, Chauhan S, Rossetti M, Font I, Basurko J, Salgado O (2010) Output-only modal analysis on operating wind turbines: application to simulated data. Presented at the European wind energy conference, Warsaw
5. Wereley NM (1991) Analysis and control of linear periodically time varying systems. PhD, Department of Aeronautics and Astronautics, Massachusetts Institute of Technology, Cambridge
6. Allen MS, Sracic MW, Chauhan S, Hansen MH (2011) Output-only modal analysis of linear time periodic systems with application to wind turbine simulation data. Mech Syst Signal Process 25:1174–1191
7. Yang S, Allen MS (2012) Output-only modal analysis using continuous-scan laser Doppler vibrometry and application to a 20 kW wind turbine. Mech Syst Signal Process 31:2011
8. Bir G (2008) Multiblade coordinate transformation and its application to wind turbine analysis. Presented at the 2008 ASME wind energy symposium, Reno
9. Skjoldan PF, Hansen MH (2009) On the similarity of the Coleman and Lyapunov-Floquet transformations for modal analysis of bladed rotor structures. J Sound Vib 327:424–439
10. Yang S, Allen MS (2012) A lifting algorithm for output-only continuous scan laser Doppler vibrometry. Presented at the AIAA, Hawaii
11. Chen C-T (1999) Linear system theory and design, 3rd edn. Oxford University Press, New York
12. Tcherniak D, Chauhan S, Hansen MH (2010) Applicability limits of operational modal analysis to operational wind turbines. Presented at the 28th international modal analysis conference (IMAC XXVIII), Jacksonville
13. Jacob T, Tcherniak D, Castiglione R (2014) Harmonic removal as a pre-processing step for operational modal analysis: application to operating gearbox data. Presented at the VDI-Fachtagung Schwingungen von Windenergieanlagen
14. Hansen MH (2004) Aeroelastic stability analysis of wind turbines using an eigenvalue approach. Wind Energy 7:133–143

15. Tcherniak D, Basurko J, Salgado O, Urresti I, Chauhan S, Carcangui CE, Rossetti M (2011) Application of OMA to operational wind turbine. Presented at the international operational modal analysis conference, Istanbul
16. Allen MS (2005) Global and Multi-Input-Multi-Output (MIMO) extensions of the Algorithm of Mode Isolation (AMI). Doctorate, George W. Woodruff School of Mechanical Engineering, Georgia Institute of Technology, Atlanta
17. Allen MS, Ginsberg JH (2006) A global, Single-Input-Multi-Output (SIMO) implementation of the algorithm of mode isolation and applications to analytical and experimental data. Mech Syst Signal Process 20:1090–1111